Model Atmosphere Analysis of Two Very Cool White Dwarfs

P. Bergeron

Département de Physique, Université de Montréal, C.P. 6128, Succ. Centre-Ville, Montréal, Québec, Canada, H3C 3J7.

and

S. K. Leggett

UKIRT, Joint Astronomy Centre, 660 North A'ohoku Place, Hilo, HI 96720.

ABSTRACT

A detailed analysis of the very cool white dwarfs SDSS 1337+00 and LHS 3250 is presented. Model atmosphere calculations with improved collision-induced absorptions by molecular hydrogen indicate that a pure hydrogen composition can be ruled out, and that the strong infrared absorption observed in these cool stars is better explained in terms of collisions of H_2 with neutral helium. It is shown that even though the overall shape of the observed energy distributions can be reproduced reasonably well with helium-rich models, the peak of the energy distribution near 6000 Å is always predicted too narrow. The extreme helium-rich composition inferred for both objects is discussed in the broader context of the extremely cool white dwarfs reported in various surveys.

Subject headings: stars: atmospheres, stars: fundamental parameters, stars: individual (SDSS 1337+00, LHS 3250), white dwarfs

1. Introduction

The photometric and spectroscopic analyses of Bergeron et al. (1997, 2001) have revealed that the coolest white dwarfs observed in the Galactic disk have effective temperatures in excess of $T_{\rm eff} \sim 4000$ K (**?**, see, e.g., Fig. 21 of)]blr01. The absence of any cooler white dwarfs can be interpreted as the result of the finite age of the disk, which has been estimated from a determination of the luminosity function at 8 ± 1.5 Gyr (Leggett et al. 1998). This value is also consistent with the location of white dwarfs in a mass versus effective temperature diagram in which theoretical isochrones are overplotted (**?**, see Figs. 24 and 25 of)]blr01.

Since the Galactic halo is believed to have formed many Gyr earlier than the disk, white dwarfs associated with the halo could be considerably older and thus cooler than those found in the disk. In addition, halo white dwarfs could be easily identified by their peculiar kinematics. This was first recognized by Liebert et al. (1989) who identified 6 white dwarfs in their luminosity function sample that had tangential velocities consistent with a halo population ($v_{\rm tan} \gtrsim 250$ km s^{-1}). Several objects from that small sample are now believed to be too young (they are too warm and massive) to belong to the Galactic halo, however (Fontaine et al. 2001).

More recently, white dwarfs with effective temperatures below 4000 K have been identified in various surveys (Hambly et al. 1999; Harris et al. 1999; Ibata et al. 2000; Harris et al. 2001; Oppenheimer et al. 2001a,b; Ruiz & Bergeron 2001; Scholz et al. 2002; Farihi et al. 2002), many of which are believed to be associated with the halo population. Even though the model fluxes are successful at reproducing in detail the optical and infrared broadband photometric observations of white dwarfs above 4000 K (Bergeron et al. 1997, 2001), the observed energy distributions of cooler white dwarfs are at odds with the predictions of model atmosphere calculations. For instance, the analysis of LHS 3250 by Harris et al. (1999) has shown that the observed optical and infrared energy distribution could not be reproduced adequately in terms of a pure hydrogen atmosphere, or a mixed hydrogen and helium composition. Similar conclusions were reached by Oppenheimer et al. (2001b). For WD 0346+246 (also analyzed by Oppenheimer et al.), Bergeron (2001) was even forced to introduce an *ad hoc* source of opacity to reproduce the observed photometry at B, V, and R.

SDSS 1337+00 is another extremely cool white dwarf discovered by Harris et al. (2001) in imaging data from the Sloan Digital Sky Survey. The optical and near-infrared spectrum of this object resemble that of LHS 3250 (**?**, see Fig. 3 of)]harris01. Photometric observations reported by Harris et al. covered only the optical $BVRI$ and a lower limit on the infrared J magnitude. In this paper, we report new infrared photometric observations at J and H for SDSS 1337+00, and provide a thorough analysis of this object as well as of LHS 3250, its almost identical twin. Both of these objects exhibit the strong infrared flux deficiency that results from collision-induced absorptions by molecular hydrogen. New calculations of this important source of opacity by Borysow and collaborators has led us to take a fresh look at the atmospheric properties of cool white dwarf atmospheres. In this paper, we thus explore in detail the effects of effective temperature, surface gravity, and atmospheric composition (hydrogen, helium, and heavier elements) on the predicted fluxes, and compare these emergent flux distributions with those of SDSS 1337+00 and LHS 3250.

2. Observations

The optical $BVRI$ photometric observations for LHS 3250 and SDSS 1337+00 are taken from Harris et al. (1999) and Harris et al. (2001), respectively. The infrared JHK photometry for LHS 3250 is also taken from Harris et al. (1999), while new J and H photometric observations were secured for SDSS 1337+00 on the nights of 2001 January 9th and 31st (UT) respectively, using the UFTI camera on the UK Infrared Telescope (UKIRT) on Mauna Kea Hawaii. Total observation time was 72 minutes for J and 63 minutes for H, made up in both cases of 60 second exposures in a repeated 9-position dither pattern. UKIRT Faint Standards were used to calibrate the photometry. The derived magnitudes were $J = 20.38 \pm 0.09$ and $H = 20.71 \pm 0.15$, on the Mauna Kea photometric system.

The energy distributions of SDSS 1337+00 and LHS 3250 have been converted into broadband fluxes following the prescription of Bergeron et al. (1997). These are shown in the upper two panels of Figure 1, together with the spectroscopic observations discussed in Harris et al. (2001), and kindly made available to us by H. Harris. It is clear from this comparison, at least in the case of SDSS 1337+00, that a detailed comparison of the observed fluxes with the model fluxes can only be made through broadband photometry. Any attempt to determine atmospheric parameters from spectroscopic data alone should be considered extremely dangerous and will not be attempted in this analysis. For instance, the drop in the infrared flux appears much more severe in the spectrum of SDSS 1337+00 than what is actually measured in photometry. Most likely this is due to the difficulty of determining an accurate instrumental response where throughput is low.

The lower panel of Figure 1 compares the relative energy distributions of SDSS 1337+00 and LHS 3250 normalized at the R bandpass. The resemblance of both objects is remarkable, and they will thus be considered together in the following model atmosphere analysis.

3. Model Atmosphere Analysis

Our white dwarf model atmospheres are based on the calculations of Bergeron et al. (1995), with the improvements described in Bergeron et al. (2001), Bergeron (2001), and references therein; the *ad hoc* pseudo-continuum opacity originating from the Lyman edge, introduced by Bergeron (2001) to account for some missing ultraviolet opacity, is omitted in the present calculations (see discussion in § 4). The models extend down to $T_{\rm eff} = 1500$ K, and the atmospheric composition may vary from pure hydrogen to pure helium, or any mixed hydrogen and helium compositions. Also, heavier elements can be included in the equation of state to study the indirect effects of traces of metals on the predicted fluxes.

We also make use of the latest collision-induced opacity calculations by Borysow and collaborators. In particular, we include the H_2-He calculations described in Jørgensen et al. (2000), as well as the recent H_2-H_2 opacities of Borysow et al. (2001), which up to now had been included in our models using the approximate formalism of Borysow et al. (1997). These improved calculations have a significant effect on the predicted energy distributions, especially below $T_{\rm eff} = 4000$ K, as can be appreciated from Figure **??** where we compare theoretical fluxes of our pure hydrogen models at various effective temperatures for the two sets of calculations (**?**, see also)]rohrmann02. The absorption bands near 0.8 and 1.1 μm are much more pronounced than previously estimated, and this will help resolve the ambiguity between our hydrogen- and helium-rich solutions presented below.

Prior to fitting each energy distribution in detail, we explore variations of all atmospheric parameters, as we feel that such a detailed investigation has never been carried out properly in the literature. We then attempt to fit the energy distributions of SDSS 1337+00 and LHS 3250 with those predicted from our model atmospheres using a nonlinear least-squares method (**?**, see)for details]brl97. Only $T_{\rm eff}$ and the solid angle $(R/D)^2$, where R is the radius of the star and D its distance from Earth, are considered free parameters. The value of $\log g$ is either assumed, or for LHS 3250, the distance can be obtained from the trigonometric parallax measurement of $\pi = 33.04 \pm 0.50$ mas (Harris et al. 1999), and the resulting stellar radius R converted into mass (and thus $\log g$) using evolutionary models. Throughout we rely on the C/O-core cooling sequences described in Bergeron et al. (2001) with thin and thick hydrogen layers, which are based on the calculations of Fontaine et al. (2001). At the low effective temperatures considered here, the thickness of the hydrogen layer does not affect the $\log g$ determination, only the cooling age estimates.

3.1. Pure Hydrogen Composition

The top panel of Figure **??** compares the relative energy distributions of SDSS 1337+00 and LHS 3250 normalized to unity at the R bandpass with pure hydrogen models at $\log g = 8.0$ normalized to unity at the maximum flux. This comparison shows that pure hydrogen models fail to match simultaneously the blue and infrared portions of the observed energy distributions. While the overall shape of the infrared flux distribution is qualitatively well reproduced with a model near $T_{\rm eff} \sim 2500$ K, the blue portion is predicted much too steep at that temperature. Similarly, the B and V photometry is better reproduced with the coolest model at 1500 K, but the infrared fluxes are then predicted too low.

The effects of varying the surface gravity are shown in the middle panel of Figure **??** for models at $T_{\rm eff} = 2500$ K. While the infrared fluxes are very sensitive to variations in

$\log g$, in particular near the I bandpass, the monochromatic fluxes shortward of R remain unaffected. Experiments with different effective temperatures (not shown here) indicate that it is never possible to reproduce all broadband photometric observations simultaneously with pure hydrogen models.

Saumon & Jacobson (1999) have studied the non-ideal effects of the equation of state on the atmospheric structure and broadband fluxes of pure hydrogen models (**?**, see also)]rohrmann02. In order to study these effects here, we have included the equation of state of Saumon et al. (1995) in our model calculations. Our results (not shown here) compare well with those shown in Figures 1 ($\log T$ vs $\log P$) and 3 (M_V vs $V-I$) of Saumon & Jacobson (1999). The effects on the energy distribution of a $T_{\rm eff} = 2500$ K, $\log g = 8.0$ model are illustrated in the bottom panel of Figure **??**, and they are shown to be negligible, at least in the sense that the failure of the pure hydrogen models to reproduce the observations in the two upper panels is not due to the neglect of the non-ideal effects in the equation of state.

Our formal fits to the optical and infrared photometry of SDSS 1337+00 and LHS 3250 are displayed in Figure **??** assuming a value of $\log g = 8.0$ for both stars. As discussed by Bergeron et al. (1997), when the observed energy distribution varies considerably over the filter bandpasses — which is obviously the case here — the comparison of the model fluxes with the observed fluxes must be performed by converting the model monochromatic fluxes into *average fluxes* from an integration over the transmission function of the corresponding bandpasses. While both of the monochromatic and average model fluxes are shown in Figure **??**, only the average fluxes are used in the least-square fitting technique described above. The surface gravity for LHS 3250 inferred from the trigonometric parallax measurement is well below 7.0, and our best fit at $\log g = 7.0$ is shown in Figure **??** as well; the overluminous property of LHS 3250 is discussed further below. The detailed fits shown here confirm the qualitative discussion above. *Our pure hydrogen models fail to reproduce the observed energy distribution of these two very cool white dwarfs.* In particular, the peaks of the energy distributions are predicted much narrower than observed.

3.2. Mixed Hydrogen and Helium Composition

Collision induced absorptions by molecular hydrogen may also result from collisions with neutral helium. Since cool helium-rich white dwarfs tend to have lower opacities and thus higher atmospheric pressures, the infrared flux deficiency appears at higher effective temperatures in helium-rich white dwarfs than in the pure hydrogen models considered above, as can be seen in Figure 9 of Bergeron et al. (2001) which shows pure hydrogen and helium-rich model sequences in the (V–I, V–K) two-color diagram.

The two upper panels of Figure **??** compare the relative energy distributions of SDSS 1337+00 and LHS 3250 with models at $T_{\rm eff} = 3250$ K, $\log g = 8.0$, for various atmospheric compositions, from pure hydrogen to pure helium. At that temperature, the maximum infrared absorption is reached at a hydrogen abundance of only $N({\rm H})/N({\rm He}) = 10^{-5}$ (shown in both upper panels); smaller or larger hydrogen abundances yield larger infrared fluxes. A comparison of the results shown in this figure with those of Figure **??** indicates that the helium-rich models, for a comparable infrared depression, tend to have energy peaks that are broader than in pure hydrogen models, in better agreement with the observed energy distributions of both SDSS 1337+00 and LHS 3250. Still, it is difficult even with helium-rich models to reconcile the optical and infrared energy distributions of these cool white dwarfs, as confirmed by our detailed fits discussed below.

In the bottom panel of Figure **??** we also explore the influence of traces of heavier elements on the emergent fluxes (**?**, see also)]jorgensen,ber01. Model atmospheres have been calculated by including metals in the equation-of-state only. Metal opacities are not taken into account as the main effect of the presence of heavy elements is to provide free electrons, and to increase the contribution of the He^- free-free opacity with respect to Rayleigh scattering, otherwise the dominant source of opacity in pure helium models (**?**, see also)]provencal02. In this particular experiment, we consider only calcium, the most common metal observed in DZ stars. These results indicate that the shape of the energy distribution is quite sensitive to the presence of heavier elements in the atmosphere. If these cool white dwarfs do have extreme helium-rich compositions, as suggested below, the presence of metals could affect significantly the atmospheric parameter determination.

Our formal fits to the photometric observations of SDSS 1337+00 and LHS 3250 using helium-rich models are shown in Figure **??**, again assuming $\log g = 8.0$ for both stars. While those fits are somewhat better than those shown in Figure **??**, they are not perfect, and certainly not as convincing as those shown in Bergeron et al. (1997) or Bergeron et al. (2001) for white dwarfs only a few hundreds of degrees warmer. The peaks of the energy distributions are still predicted too sharp, and the flux in the R band is always overestimated. Experiments with models including metals have not improved the quality of the fits, and will not be discussed further. Our best fit to LHS 3250 using the trigonometric parallax measurement is also displayed in Figure **??**, and yields a value of $\log g = 7.27$, or a mass of only 0.23 $M_\odot$. Such a low-mass would imply in turn that LHS 3250 has a helium core — the product of close binary evolution. However, this interpretation is at odds with the spectroscopic mass distributions of DA and DB stars by Bergeron et al. (1992) and Beauchamp et al. (1996), respectively, and the photometric analysis of cool white dwarfs with trigonometric parallax measurements by Bergeron et al. (2001), which indicate that low mass white dwarfs all have hydrogen-rich atmospheres.

Our best solutions for LHS 3250 with pure hydrogen or mixed hydrogen/helium compositions are contrasted in Figure **??**, and compared with the optical spectrum. While none of our fits reproduce the observations perfectly, the optical spectrum allows us to rule out the pure hydrogen solution since the deep absorption feature near 0.8 μm is clearly not observed. We note that calculations with the earlier collision-induced H_2 opacities of **?**)][not shown here]borysow97 precluded us from reaching such a conclusion because the depth of the molecular bands were not predicted as deep (see Figure **??**). We are now able to conclude with our latest model grid that both SDSS 1337+00 and LHS 3250 are better explained in terms of extreme helium-rich compositions, despite the fact that our current model atmospheres do not yield perfect fits to the observed photometry.

Another argument in favor of the helium-rich solution is the overluminosity problem for LHS 3250 discussed earlier with the pure hydrogen models. This is best illustrated in Figure **??** where we show the location of LHS 3250 in a M_V vs (V–I) color-magnitude diagram together with pure hydrogen and N(H)/N(He) = 10^{-5} models at $\log g$ = 8.0. While it is clearly impossible to reconcile the observed luminosity of LHS 3250 with pure hydrogen models, the helium-rich sequence is more consistent with the location of LHS 3250 in this diagram. Lower gravity (larger radii and thus larger luminosity) models would improve the agreement even further, as indicated in Figure **??** where we show the predicted values of M_V and (V–I) obtained from our best solution at $\log g = 7.27$ shown in the lower panel of Figure **??**.

The overluminosity of LHS 3250 may also suggest that these stars are unresolved degenerate binaries. We have also attempted to fit the observed energy distributions with two white dwarf models, weighted by their respective radius. Despite the large number of free parameters in the possible solutions, the best fits achieved are not better than those shown in Figures **??** or **??** and thus were not considered further.

Finally we show in Figure **??** the location of SDSS 1337+00 and LHS 3250 in a (V–I, V–H) two-color diagram, together with theoretical colors from model atmospheres with various chemical compositions. Also shown are the photometric data from the cool white dwarf sample of Bergeron et al. (1997, 2001), as well as the photometry of WD 0346+246, the low luminosity white dwarf discovered by Hambly et al. (1997). The variation of helium abundances is illustrated by the sequence at $T_{\rm eff}$ = 3250 K, which performs an excursion from the pure hydrogen to a pure helium composition, reaching minimum values of V–I and V–H at N(H)/N(He) $\sim 10^{-5}$. In this diagram, SDSS 1337+00 is consistent with the helium-rich solution while LHS 3250 is marginally consistent with both solutions. The location of the cool white dwarf WD 0346+246 also suggests a helium-rich composition (see discussion below).

4. Discussion

The extreme helium-rich composition inferred in our analysis for both SDSS 1337+00 and LHS 3250 poses an obvious and challenging problem. Because the outer layers of cool white dwarfs are strongly convective, the hydrogen and helium chemical composition tends to be more or less homogeneous throughout the mixed convection zone. Since below $T_{\rm eff} \sim 12,000$ K, the mass of the deep helium convection zone is almost constant at $M_{\rm He-conv} \sim 10^{-6}\ M_*$ (Tassoul et al. 1990), the small hydrogen abundances of only $N({\rm H})/N({\rm He}) \sim 10^{-5} - 10^{-4}$ derived in our analysis imply a *total* hydrogen mass of $\sim 5 \times 10^{-12}\ M_\odot$. If this amount of hydrogen has been accreted from the interstellar medium over a cooling age of roughly 10 Gyr for a 3500 K white dwarf, the implied accretion rate would be only $\sim 10^{-22}\ M_\odot\ {\rm yr}^{-1}$, a value that is completely unrealistic. For instance, the theoretical estimates of Wesemael (1979) suggest time-averaged accretion rates of $\sim 10^{-17}\ M_\odot\ {\rm yr}^{-1}$. Of course, the extreme helium-rich compositions derived here for SDSS 1337+00 and LHS 3250 cannot be completely ruled out on the basis of these arguments alone since the problem of the accretion of hydrogen in cool white dwarfs is a long standing one, and no satisfactory explanation has yet been proposed to account for the persistence of helium-rich white dwarfs at low effective temperatures.

We note in this context that WD 0346+246 shown in Figure **??** has been interpreted by Oppenheimer et al. (2001b) as a $T_{\rm eff} = 3750$ K white dwarf with an extremely small hydrogen abundance of $\log N({\rm H})/N({\rm He}) = -6.4$. A reanalysis of this object by Bergeron (2001) with the improved H_2-He collision-induced opacities of Jørgensen et al. (2000) indicates an even lower hydrogen abundance of $N({\rm H})/N({\rm He}) \sim 10^{-9}$. Because this solution was improbable — but not impossible — from accretion considerations, Bergeron (2001) proposed an alternative solution with a higher hydrogen abundance of $N({\rm H})/N({\rm He}) \sim 0.8$, but was also forced to introduce in the model calculations a bound-free opacity from the Lyman edge associated with the so-called dissolved atomic levels of the hydrogen atom, in order to reduce the near-UV flux and match the optical photometric observations. This additional pseudo-continuum opacity has not been included in the present calculations as the UV flux is already predicted too low for SDSS 1337+00 and LHS 3250.

While it is probably safe to conclude that these cool white dwarfs have helium-rich atmospheres and effective temperatures below 4000 K, it is not yet possible to determine their atmospheric parameters and ages with great precision since the models fail to reproduce the photometric observations in detail. The large parameter space explored in our analysis suggests that the source of this discrepancy lies in the physics included in our model atmospheres, which is either inadequate or incomplete. One avenue of investigation worth considering is non-ideal effects of the equation-of-state at the high atmospheric pressures

that characterize helium-rich atmospheres. So far, these effects have only been estimated in pure hydrogen or pure helium atmospheres (**?**)this paper]bsw95,saumon99,rohrmann02. It has also been demonstrated recently by Iglesias et al. (2002) that the helium free-free opacity and Rayleigh scattering at high densities typical of those encountered here are seriously overestimated. The use of their improved treatment in model atmosphere calculations would most likely increase the flux where the collision-induced opacity is less important, i.e. for wavelengths below 0.7 μm, precisely in the region where we observe the largest discrepancy. This could even solve the overluminosity problem of LHS 3250 altogether as the calculated absolute visual magnitude for helium-rich white dwarfs would be brighter.

All white dwarfs below $T_{\rm eff} = 4000$ K for which a detailed analysis has been performed have been explained in terms of some mixed hydrogen and helium atmospheric compositions, or even a pure helium composition (**?**)]harris99,opp01b,ber01,farihi02. There are still no white dwarfs below $T_{\rm eff} = 4000$ K that have been successfully and convincingly explained in terms of a pure hydrogen atmospheric composition. This result may not be completely unexpected since helium-atmosphere white dwarfs with their lower opacities have cooling time scales that can be considerably shorter than their hydrogen-atmosphere counterparts (**?**, see, e.g.,)]hansen99, blr01. Hence for a given population and at a given mass, the coolest white dwarfs are expected to have helium-dominated atmospheres. For instance, a cool helium-rich white dwarf at $T_{\rm eff} = 3250$ K (i.e., our temperature estimate for SDSS 1337+00) with an average mass of $\sim 0.7\ M_{\odot}$ (**?**, see Fig. 22 of)]blr01 has a cooling age of only 9.4 Gyr according to our evolutionary models with thin hydrogen layers (**?**, see also Fig. 24 of)]blr01; by comparison, a similar object with a thick hydrogen layer would have an age of 11.6 Gyr. This 9.4 Gyr estimate is entirely consistent with the age of the oldest objects in the Galactic disk analyzed by Bergeron et al. (2001), and the so-called ultracool white dwarfs reported in the literature may not be terribly old after all. Although WD 0346+246 has kinematics supporting halo membership (Hambly et al. 1999), LHS 3250 has a lower tangential velocity consistent with membership of either disk or halo, and SDSS 1337+00 has an even lower velocity inconsistent with halo membership (Harris et al. 2001).

Despite the fact that we do not fully understand the accretion mechanism in cool white dwarfs, helium-atmosphere white dwarfs must eventually accrete "some amount" of hydrogen, at which point they will exhibit a strong infrared flux deficiency, even if the amount of hydrogen is extremely small according to our calculations. SDSS 1337+00 and LHS 3250 are most likely such objects, and extremely cool hydrogen-atmosphere white dwarfs belonging to the old halo population of the Galaxy are yet to be identified.

We are grateful to H. Harris for providing us with the spectra of SDSS 1337+00 and LHS 3250. This work was supported in part by the NSERC Canada and by the Fund NATEQ

(Québec). The J and H magnitudes for SDSS 1337+00 were obtained through the UKIRT Service Programme. UKIRT, the United Kingdom Infrared Telescope, is operated by the Joint Astronomy Centre on behalf of the U.K. Particle Physics and Astronomy Research Council.

REFERENCES

Beauchamp, A., Wesemael, F., Bergeron, P., Liebert, J., & Saffer, R. A. 1996, in ASP Conf. Ser. Vol. 96, Hydrogen-Deficient Stars, ed. S. Jeffery & U. Heber (San Francisco: ASP), 295

Bergeron, P. 2001, ApJ, 558, 369

Bergeron, P., Leggett, S. K., & Ruiz, M. T. 2001, ApJS, 133, 413

Bergeron, P., Ruiz, M. T., & Leggett, S. K. 1997, ApJS, 108, 339

Bergeron, P., Saffer, R. A., & Liebert, J. 1992, ApJ, 394, 228

Bergeron, P., Saumon, D., & Weseamel, F. 1995, ApJ, 443, 764

Borysow, A., Jørgensen, U. G., & Fu, Y. 2001, J. Quant. Spec. Radiat. Transf., 68, 235

Borysow, A., Jørgensen, U. G., & Zheng, C. 1997, A&A, 324, 185

Farihi, J., Becklin, E. E., & Zuckerman, B. 2002, ApJ, submitted

Fontaine, G., Brassard, P., & Bergeron, P. 2001, PASP, 113, 409

Hambly, N. C., Smartt, S. J., & Hodgkin, S. T. 1997, ApJ, 489, L157

Hambly, N. C., Smartt, S. J., Hodgkin, S. T., Jameson, R. F., Kemp, S. N., Rolleston, W. R. J., & Steele I. A. 1999, MNRAS, 309, L33

Hansen, B. M. S. 1999, ApJ, 520, 680

Harris, H. C., Dahn, C. C., Vrba, F. J., Henden, A. A., Liebert, J., Schmidt, G. D., & Reid, I. N. 1999, ApJ, 524, 1000

Harris, H. C., et al. 2001, ApJ, 549, L109

Ibata, R., Irwin, M., Bienaymé, O., Scholz, R., & Guibert, J. 2000, ApJ, 532, L41

Iglesias, C. A., Rogers, F. J., & Saumon, D. 2002, ApJ, 569, L111

Jørgensen, U. G., Hammer, D., Borysow, A., & Falkesgaard, J. 2000, A&A, 361, 283

Leggett, S. K., Ruiz, M. T., & Bergeron, P. 1998, ApJ, 497, 294

Liebert, J., Dahn, C. C., & Monet, D. G. 1989, in IAU Colloq. 114, White Dwarfs, ed. G. Wegner (Berlin: Springer), 15

Oppenheimer, B. R., Hambly, N. C., Digby, A. P., Hodgkin, S. T., & Saumon, D. 2001a, Science, 292, 698

Oppenheimer, B. R., Saumon, D., Hodgkin, S. T., Jameson, R. F., Hambly, N. C., Chabrier, G., Filipenko, A. V., Coil, A. L., & Brown, M. E. 2001b, ApJ, 550, 448

Provencal, J. L., Shipman, H. L., Koester, D., Wesemael, F., & Bergeron, P. 2002, ApJ, 568, 324

Rohrmann, R., Serenelli, A. M., Althaus, L. G., & Benvenuto, O. G. 2002, MNRAS, in press

Ruiz, M. T., & Bergeron, P. 2001, ApJ, 558, 761

Saumon, D., Chabrier, G., & Van Horn, H. M. 1995, ApJS, 99, 713

Saumon, D., & Jacobson, S. B. 1999, ApJ, 511, L107

Scholz, R.-D., Szokoly, G. P., Andersen, M., Ibata, R., & Irwin, M. J. 2002, ApJ, 565, 539

Tassoul, M., Fontaine, G., & Winget, D. E. 1990, ApJS, 72, 335

Wesemael, F. 1979, A&A, 72, 104

AAS LaTeX macros v5.0.

Fig. 1.— Upper panels: Optical $BVRI$ and infrared JHK photometry of SDSS 1337+00 and LHS 3250 displayed as broadband fluxes (with corresponding error bars) following the prescription of **?**)][]brl97; only J and H have been measured for SDSS 1337+00. Also shown for comparison are the spectroscopic observations for each object taken from Harris et al. (2001). Bottom panel: Comparison of the energy distributions of both stars normalized to unity at R.
1214.5

1214.5

[

dotted lines]borysow97 and [

solid lines]borysow01. For each effective temperature (the leftmost model is at $T_{\rm eff}$ = 2000 K), the fluxes are normalized to unity at the maximum flux of the Borysow et al. (2001) models.13

Comparison of emergent fluxes from our pure hydrogen model atmospheres using the collision-induced opacity calculations of **?**)][dotted lines]borysow97 and **?**)][solid lines]borysow01. For each effective temperature (the leftmost model is at $T_{\rm eff}$ = 2000 K), the fluxes are normalized to unity at the maximum flux of the Borysow et al. (2001) models.

Fig. 3.— Relative energy distributions of SDSS 1337+00 and LHS 3250 normalized to unity at the R bandpass compared with various pure hydrogen models normalized to unity at the maximum flux. The top panel compares models at $\log g$ = 8.0 with $T_{\rm eff}$ = 1500 K (solid line) to 3000 K by step of 500 K. The middle panel compares models at $T_{\rm eff}$ = 2500 K with $\log g$ = 7.0 (solid line) to 9.0 by step of 0.5. The bottom panel compares models at $T_{\rm eff}$ = 2500 K, $\log g$ = 8.0 calculated with an ideal equation of state, as well as with the non-ideal equation of state of Saumon et al. (1995).

Fig. 4.— Fits to the energy distributions of SDSS 1337+00 and LHS 3250 with pure hydrogen models. The optical $BVRI$ and infrared $JH(K)$ photometric observations are shown by the error bars. The solid lines correspond to the model monochromatic fluxes at $\log g$ = 8.0, while the filled circles represent the average over the filter bandpasses. For LHS 3250, our best fit at $\log g$ = 7.0 is shown as the dotted line and open circles.

Fig. 5.— Relative energy distributions of SDSS 1337+00 and LHS 3250 normalized to unity at the R bandpass compared with various mixed hydrogen/helium/calcium models normalized to unity at the maximum flux. The top panel compares models at $T_{\rm eff}$ = 3250 K

and $\log g = 8.0$ from a pure hydrogen composition (solid line) to a value of $N(\mathrm{He})/N(\mathrm{H}) = 10^5$ where the infrared flux deficiency is the strongest. In the middle panel, the hydrogen abundance is further decreased from a value of $N(\mathrm{H})/N(\mathrm{He}) = 10^{-5}$ (solid line) to a pure helium composition. In the bottom panel, the helium abundance is fixed but the calcium abundance is varied.

Fig. 6.— Fits to the energy distributions of SDSS 1337+00 and LHS 3250 with pure helium-rich models. The various symbols are explained in Figure **??**. The fit for LHS 3250 shown as the dotted line and open circles relies on the trigonometric parallax measurement.

Fig. 7.— Comparison of the best solutions for LHS 3250 under the assumption of a pure hydrogen composition (*solid line*) and a mixed hydrogen/helium composition (*dotted line*). Also shown are the broadband photometry and optical spectrum. The latter suggests that LHS 3250 has a helium-rich composition rather than a pure hydrogen atmosphere.

Fig. 8.— Location of LHS 3250 in the M_V vs (V–I) color-magnitude diagram; the size of the solid dot corresponds to the error of M_V. The open circles represent the photometric data taken from Bergeron et al. (2001). The model sequences correspond to $\log g = 8.0$ models for pure hydrogen and $N(\mathrm{H})/N(\mathrm{He}) = 10^{-5}$ atmospheric compositions. The small dots on each sequence are separated by $\Delta T_{\rm eff} = 250$ K, and effective temperatures are indicated in units of 10^3 K. The plus sign indicates the location of our best solution at $\log g = 7.27$ shown in the lower panel of Figure **??**.

Fig. 9.— Location of SDSS 1337+00 and LHS 3250 in the (V–I, V–H) two-color diagram. Also shown are the cool white dwarf photometric observations taken from Bergeron et al. (1997, 2001), and the photometry of WD 0346+246 from Oppenheimer et al. (2001b). The theoretical colors shown as solid lines correspond to pure hydrogen models (He/H = 0), pure helium models (H/He = 0), and mixed hydrogen and helium compositions (H/He = 10^{-5}) at various effective temperatures, all at $\log g = 8.0$; on each sequence the plus signs are separated by $\Delta T_{\rm eff} = 250$ K, starting at $T_{\rm eff} = 6000$ K on the observed photometric sequence. The dotted line corresponds to a $T_{\rm eff} = 3250$ K, $\log g = 8.0$ model sequence for various helium abundances; the plus signs are separated by 1 dex in $\log N(\mathrm{He})/N(\mathrm{H})$, starting at $N(\mathrm{He})/N(\mathrm{H}) = 10^{-2}$ near the pure hydrogen sequence.

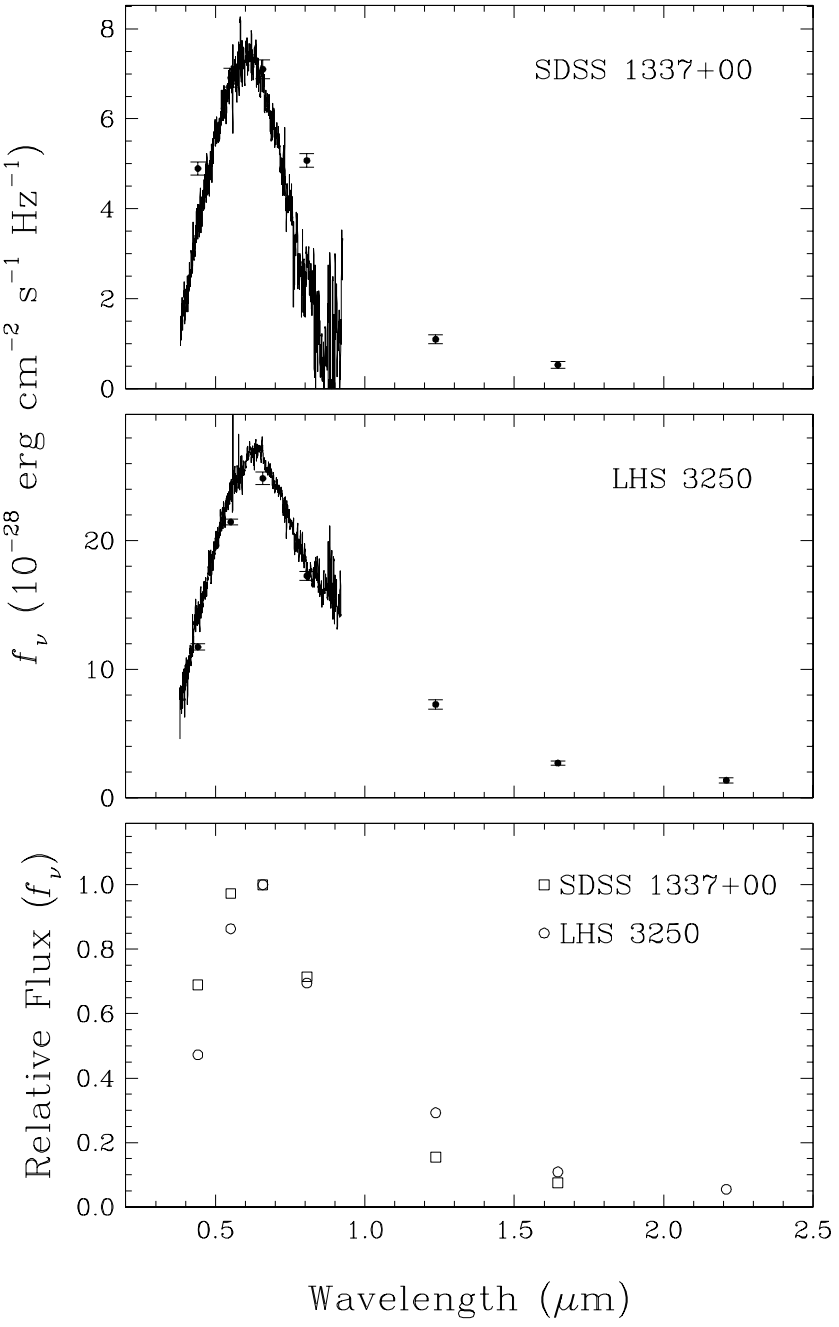
SDSS 1337+00
LHS 3250
f_ν (10^{-28} erg cm^{-2} s^{-1} Hz^{-1})
Relative Flux (f_ν)
SDSS 1337+00
LHS 3250
Wavelength (μm)

Figure 1

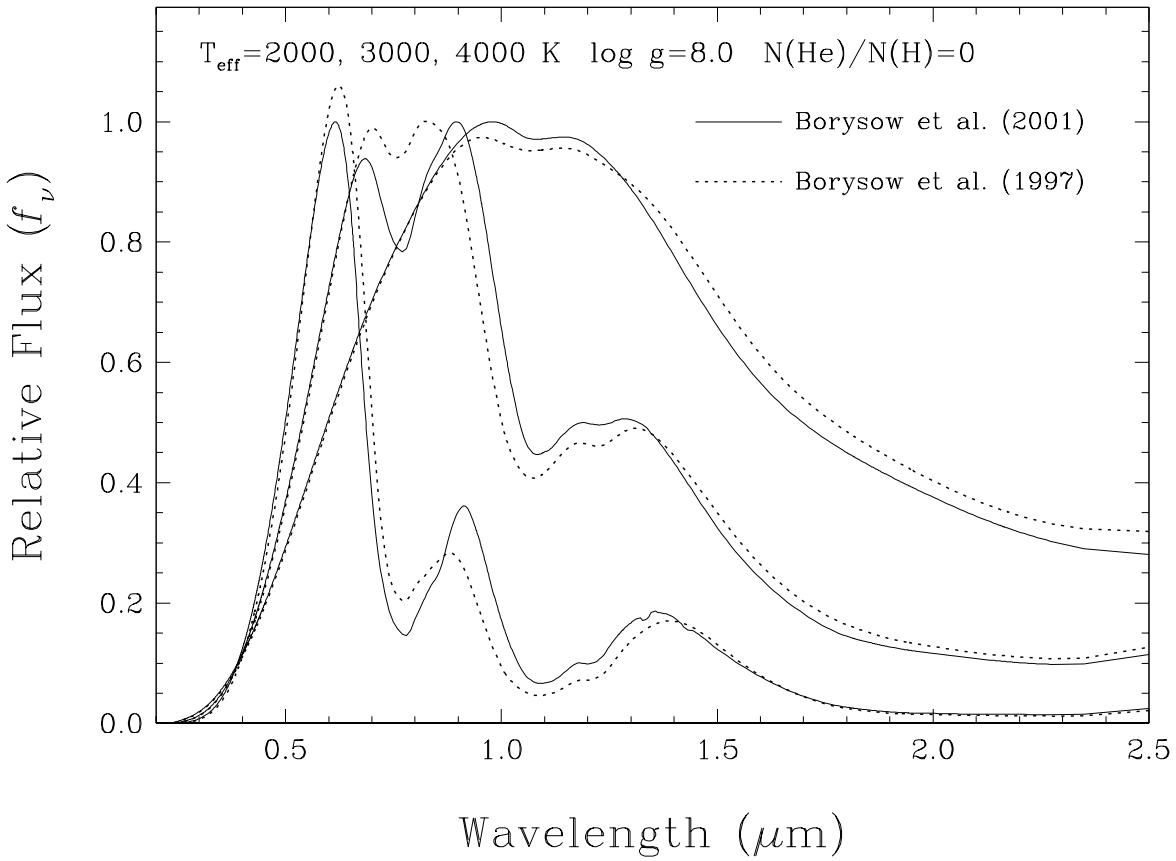
T_eff=2000, 3000, 4000 K log g=8.0 N(He)/N(H)=0
Borysow et al. (2001)
Borysow et al. (1997)
Relative Flux (f_ν)
Wavelength (μm)
0.0
0.2
0.4
0.6
0.8
1.0
0.5
1.0
1.5
2.0
2.5

Figure **??**

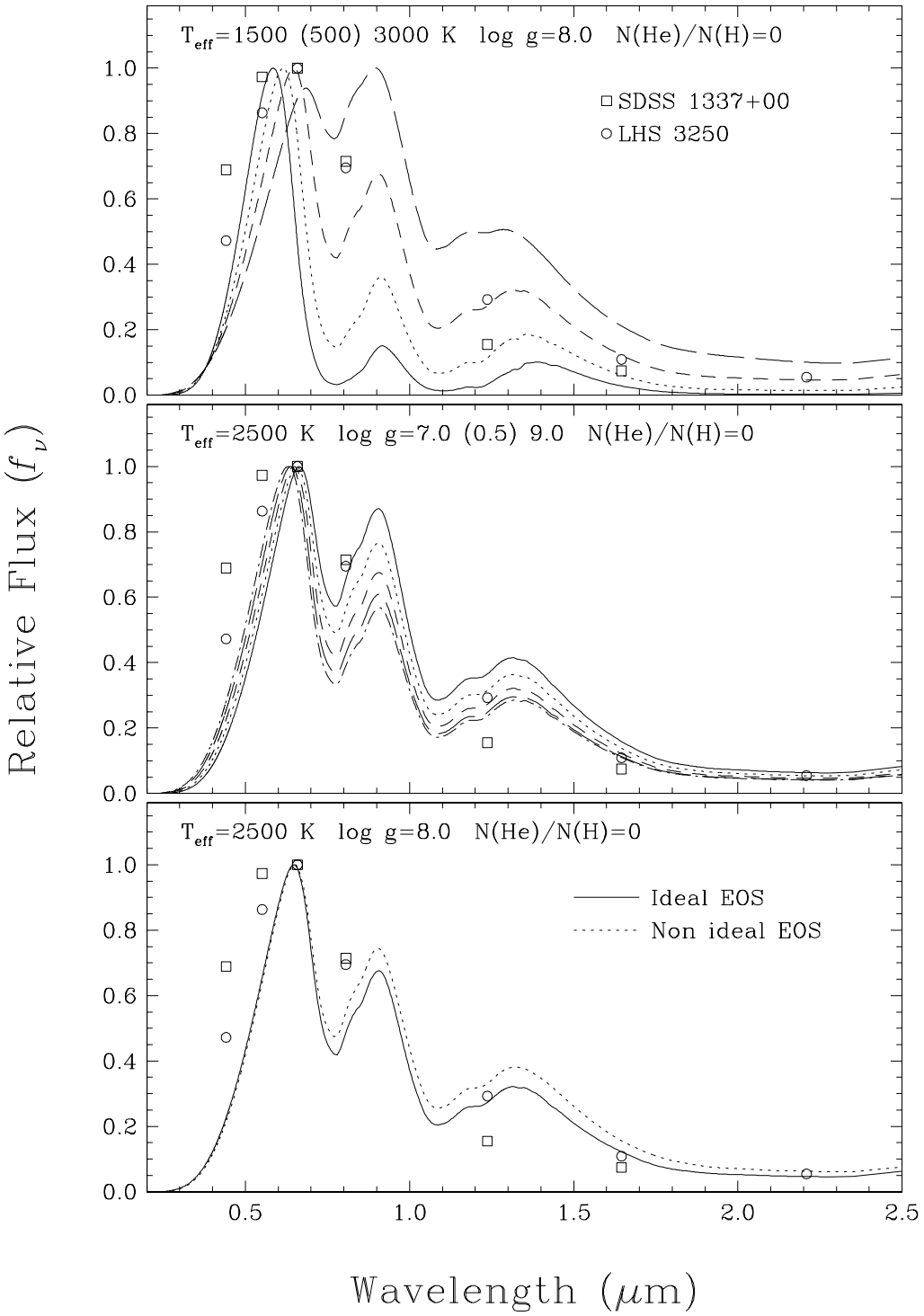
T_eff=1500 (500) 3000 K log g=8.0 N(He)/N(H)=0
SDSS 1337+00
LHS 3250
T_eff=2500 K log g=7.0 (0.5) 9.0 N(He)/N(H)=0
T_eff=2500 K log g=8.0 N(He)/N(H)=0
Ideal EOS
Non ideal EOS
Relative Flux (f_ν)
Wavelength (μm)

Figure **??**

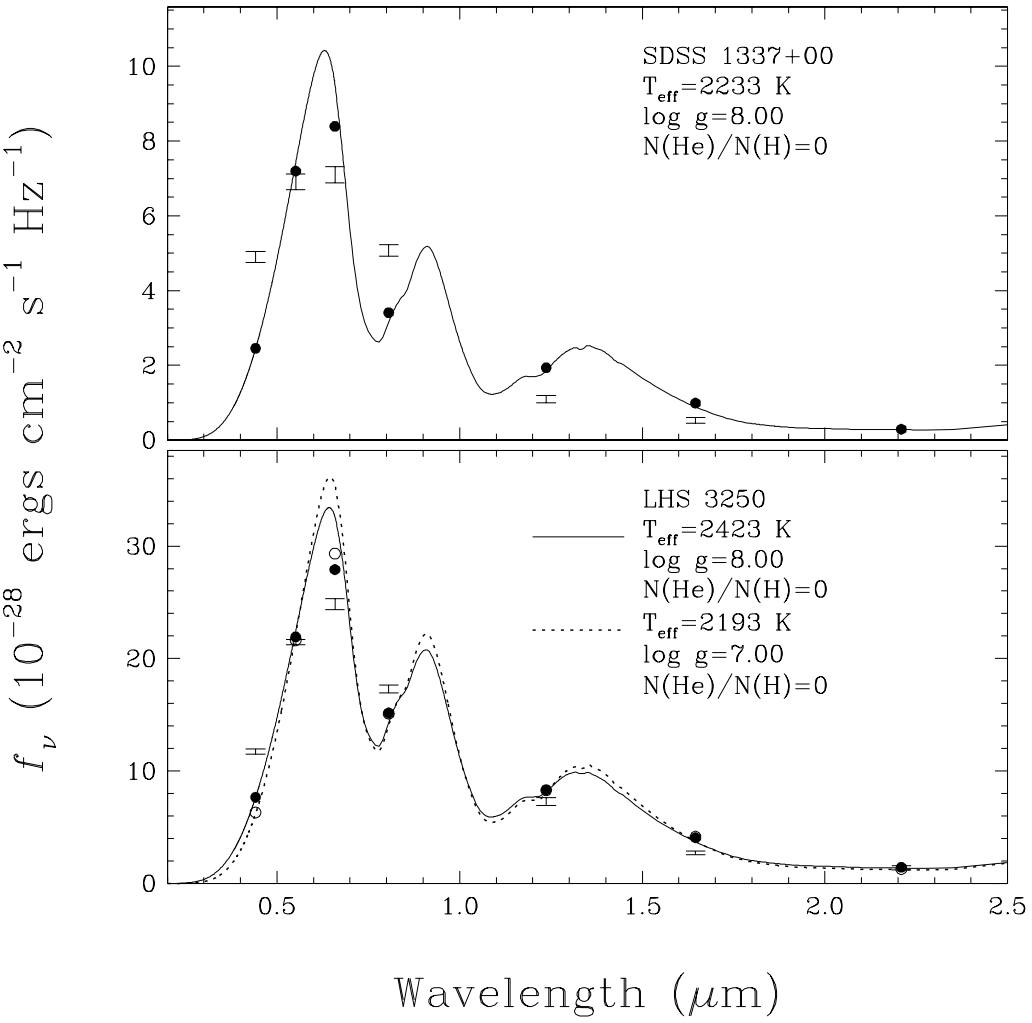
SDSS 1337+00
T_eff=2233 K
log g=8.00
N(He)/N(H)=0
LHS 3250
T_eff=2423 K
log g=8.00
N(He)/N(H)=0
T_eff=2193 K
log g=7.00
N(He)/N(H)=0
f_ν (10^-28 ergs cm^-2 s^-1 Hz^-1)
Wavelength (μm)

Figure **??**

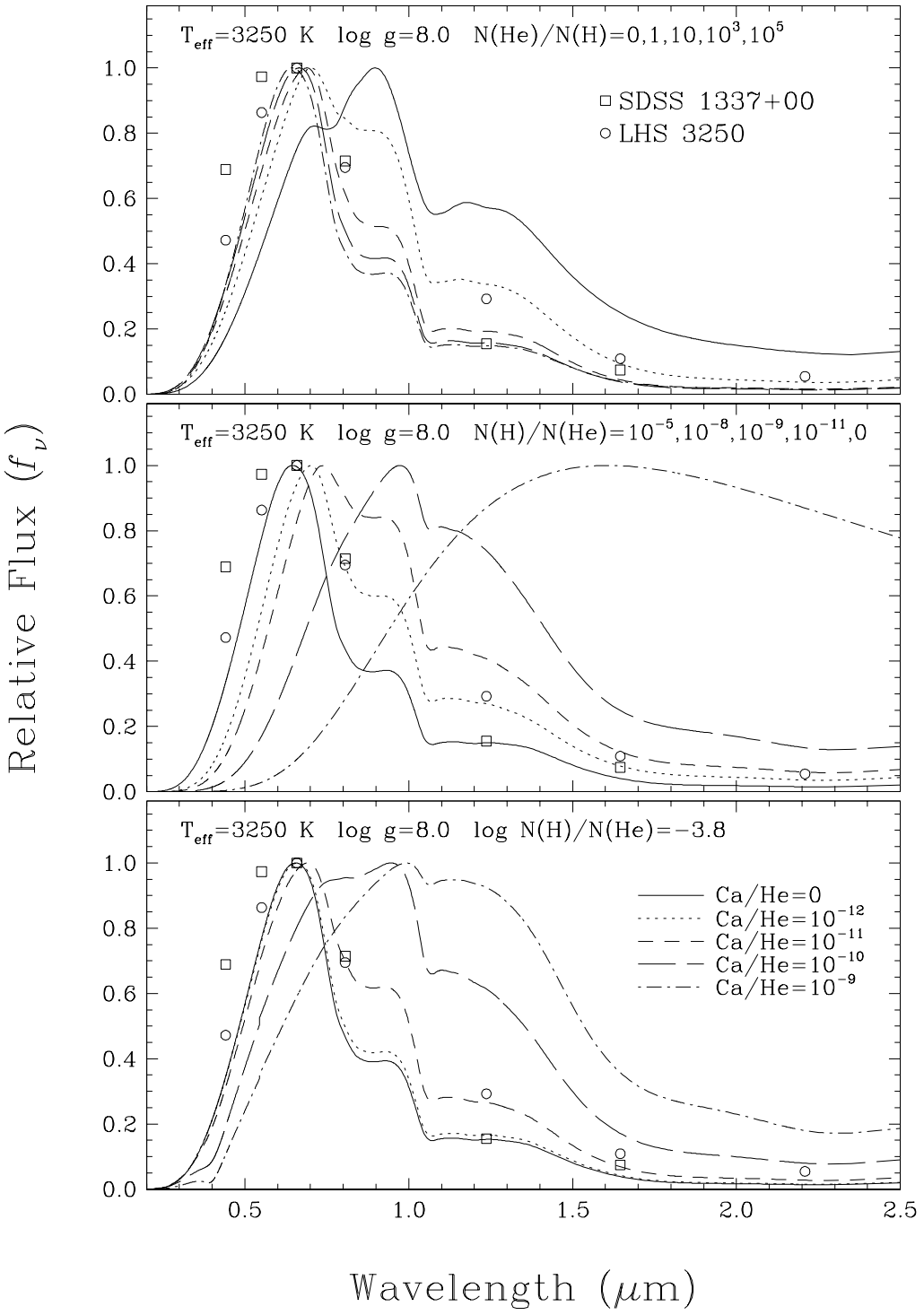
T_eff=3250 K log g=8.0 N(He)/N(H)=0,1,10,10^3,10^5
SDSS 1337+00
LHS 3250
T_eff=3250 K log g=8.0 N(H)/N(He)=10^-5,10^-8,10^-9,10^-11,0
T_eff=3250 K log g=8.0 log N(H)/N(He)=−3.8
Ca/He=0
Ca/He=10^-12
Ca/He=10^-11
Ca/He=10^-10
Ca/He=10^-9
Relative Flux (f_ν)
Wavelength (μm)
0.0
0.2
0.4
0.6
0.8
1.0
0.5
1.0
1.5
2.0
2.5

Figure **??**

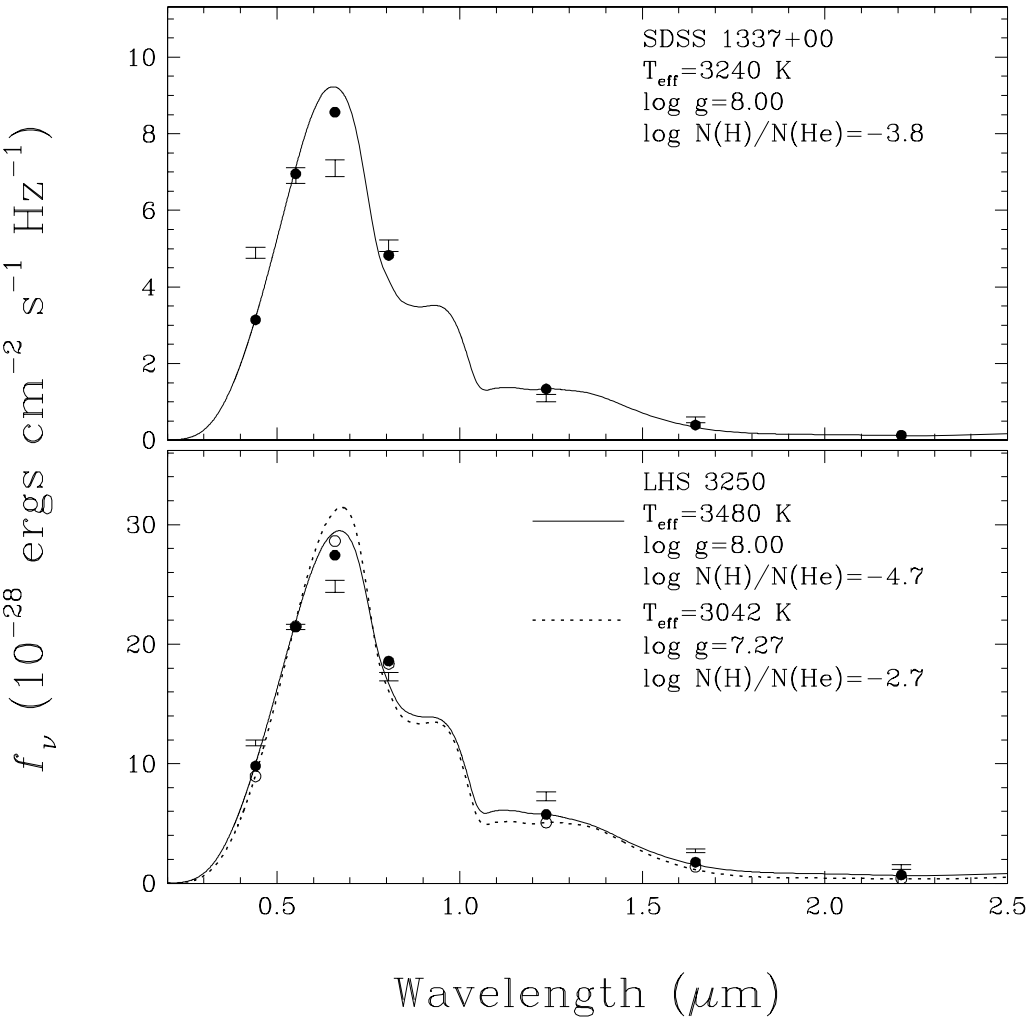
SDSS 1337+00
T_eff=3240 K
log g=8.00
log N(H)/N(He)=−3.8
LHS 3250
T_eff=3480 K
log g=8.00
log N(H)/N(He)=−4.7
T_eff=3042 K
log g=7.27
log N(H)/N(He)=−2.7
f_ν (10^−28 ergs cm^−2 s^−1 Hz^−1)
Wavelength (μm)

Figure **??**

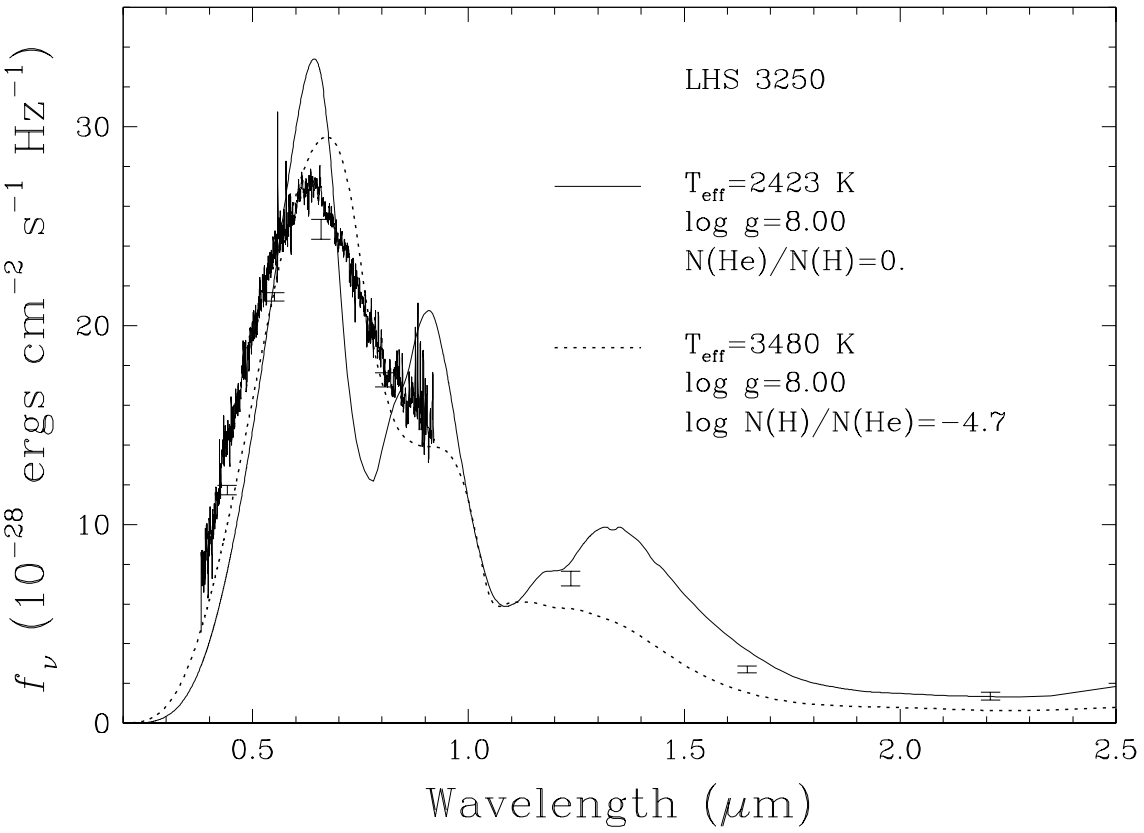
LHS 3250
T_eff=2423 K
log g=8.00
N(He)/N(H)=0.
T_eff=3480 K
log g=8.00
log N(H)/N(He)=−4.7
f_ν (10^−28 ergs cm^−2 s^−1 Hz^−1)
Wavelength (μm)
0
10
20
30
0.5
1.0
1.5
2.0
2.5

Figure **??**

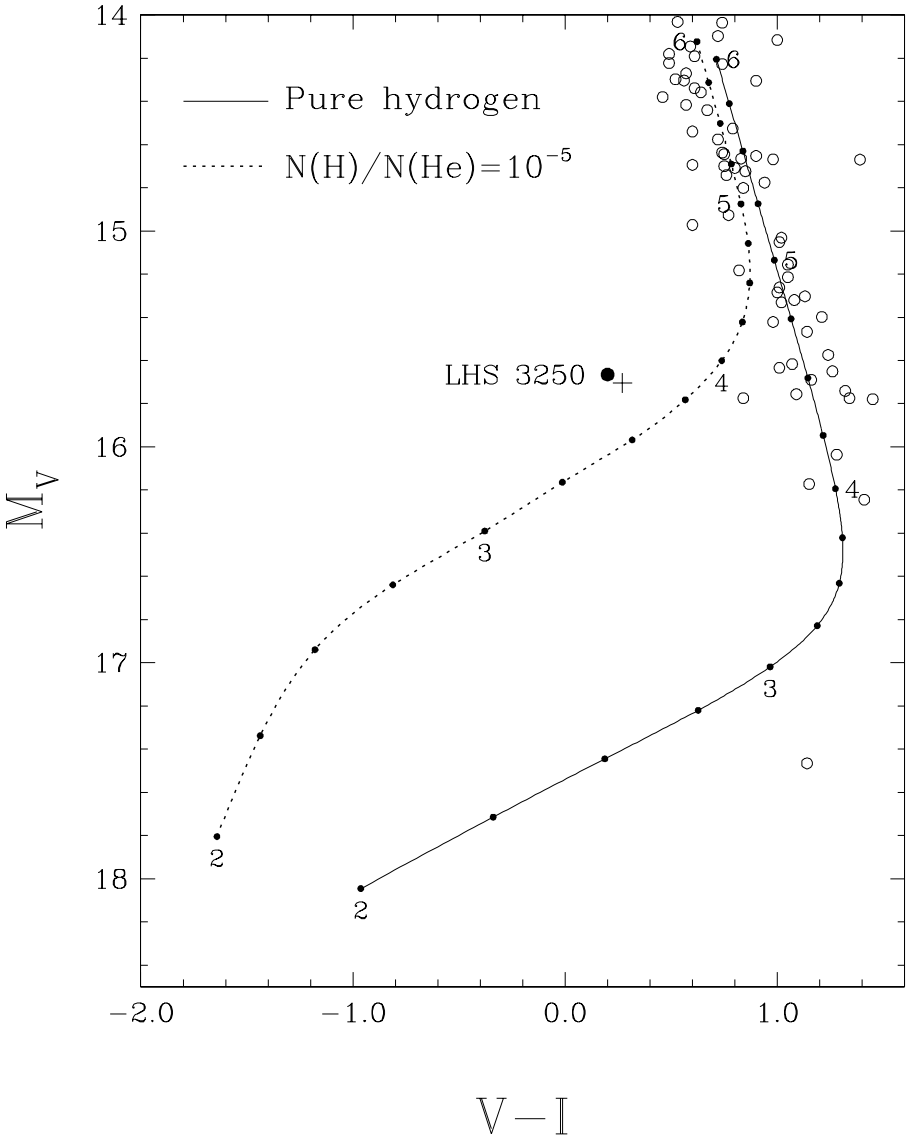
Pure hydrogen
N(H)/N(He)=10^-5
LHS 3250
M_V
V − I
14
15
16
17
18
−2.0
−1.0
0.0
1.0
2
3
4
5
6

Figure **??**

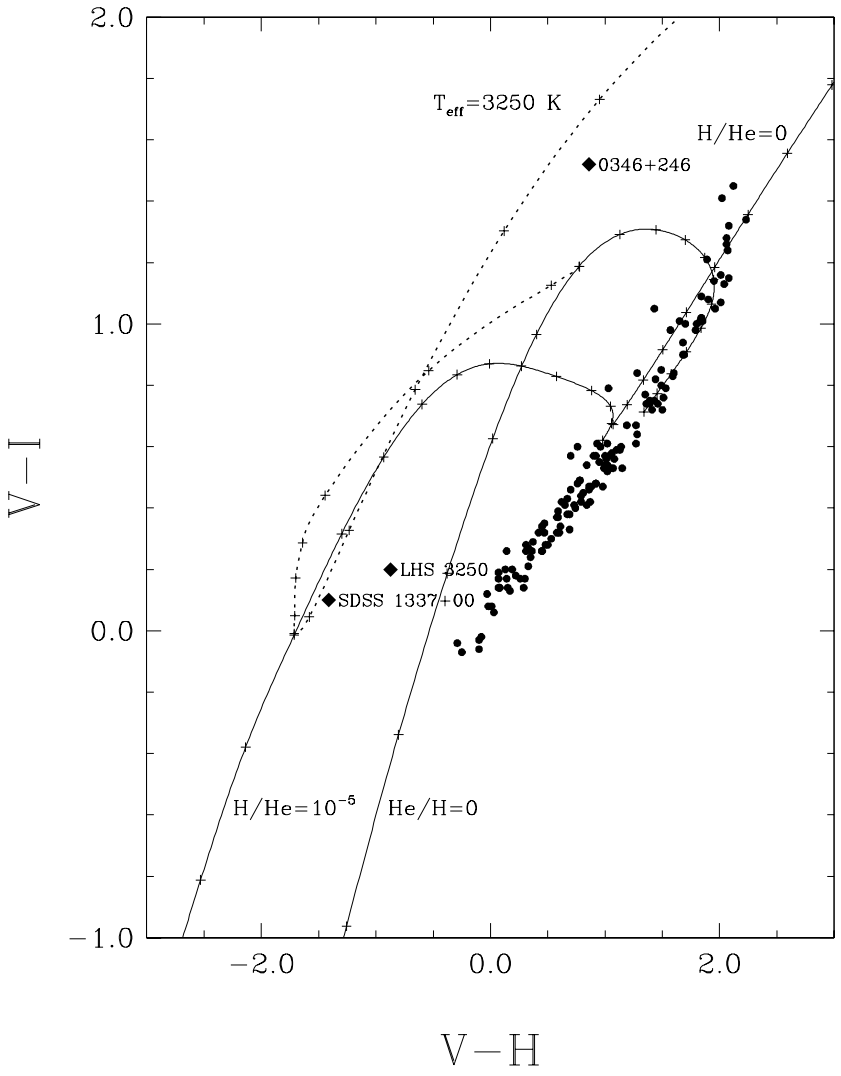
2.0
1.0
0.0
−1.0
−2.0
0.0
2.0
V−I
V−H
T$_{eff}$=3250 K
H/He=0
0346+246
LHS 3250
SDSS 1337+00
H/He=10^{-5}
He/H=0

Figure ??